IEEE Access
Multidisciplinary | Rapid Review | Open Access Journal

IEEE MAGNETICS SOCIETY SECTION

Received 5 July 2024, accepted 12 August 2024, date of publication 16 August 2024, date of current version 27 August 2024.

Digital Object Identifier 10.1109/ACCESS.2024.3445168

METHODS

Optimization of Solenoid Parameters for a Magnetic Nozzle Assembly Using Design of Experiments

CHRISTOPH PETER AND MARTIN TAJMAR
Institute of Aerospace Engineering, Technische Universität Dresden, 01069 Dresden, Germany
Corresponding author: Christoph Peter (christoph.peter@tu-dresden.de)

This work was supported by German Aerospace Center (DLR) under Grant 50RS2103.

ABSTRACT A method for optimizing multiple responses in solenoids utilized in a magnetic nozzle assembly for an electric plasma thruster is presented. The primary goal is to minimize power usage while maintaining a sufficiently high magnetic flux density at the coil axis. This is especially critical during testing in a vacuum chamber, where heat dissipation is a challenge, especially for small components and intricate assemblies. This paper presents a method for quickly calculating the magnetic field along the solenoid axis that provides accurate estimates, independent of coil size. Additionally, we present general and concrete results for the employed magnetic nozzle design to illustrate the applied optimization method. The paper details a methodology for optimizing multiple parameters of a solenoid, including its radius, length, current, number of turns, and wire diameter. The aim is to minimize, maximize, or meet specific targets for magnetic flux density, power, or mass. Additional studies could utilize a suitable metric to optimize the homogeneity of the magnetic field of multiple coils. The coils designed using the algorithm have a radius of 17.5 mm, a length of 21 mm, consist of 300 turns with a wire diameter of 1 mm, and operate at a direct current of about 5 A. The potential maximum magnetic field is 40 mT with a power consumption of around 30 W.

INDEX TERMS Design of experiments, magnetic nozzle, multiple response analysis, optimization, solenoid.

NOMENCLATURE

B	Magnetic flux density.
$\vec{B}$	Magnetic flux density vector.
B_{max}	Peak magnetic flux density.
d_w	Wire diameter.
$\bar{d}$	Wire gauge including coating.
F	Desirability function for optimization
H	Magnetic field strength.
Δh	Center-to-center distance between two conductor layers in the coil winding
I	Current (DC).
$k_{1...3}$	Factor of importance for desirability factors.
L	Solenoid length.
$L_{1...3}$	Optimization limit.
$d\vec{l}$	Wire element.
m	Mass.
N	Number of windings.
n_q	Number of optimization responses.
P	Power.
$q_{1...3}$	Desirability factors.
R	Radius.
$\bar{R}$	Solenoid mean radius.
R_i	Solenoid inner radius.
r	Distance from $d\vec{l}$ to observation point.
$\hat{\boldsymbol{r}}$	Unit vector of r.
$r_{1...3}$	Exponents to shape desirability factors.
$T_{1...3}$	Optimization target.
z	Vertical distance.
θ	Angle between $\vec{B}$ and its horizontal component.
μ_0	Vacuum magnetic permeability.

The associate editor coordinating the review of this manuscript and approving it for publication was Valentine Novosad.

I. INTRODUCTION

Solenoids are widely used in industry and science as variable magnetic field sources or induction coils. Their use as a

magnetic field source requires an accurate knowledge of the resulting flux density and thus an equally accurate design of the coil parameters such as number of turns, coil radius, length and current, which all determine the magnetic field strength.

Over the years, many researchers have studied solenoids for various applications and use cases. Studies aimed at optimization have mainly focused on solenoid actuators due to their numerous applications but complex modeling and design [1], [2], [3], [4], [5], [6], [7]. Recent work uses genetic algorithms to optimize the design and response of electromagnetic actuators. Mach et al. [8] use it for geometric optimization of the plunger of an actuator. Hey et al. [9] developed a two-step algorithm for global optimization of an actuator in terms of achievable force per unit heat dissipation. In addition, parametric studies are also used for design, e.g. by Lalitha and Gupta [10] to design a high-temperature superconducting coil. Similar to Mach et al. [8], Plavec and Vidovic [11] also use genetic algorithms for shape optimization. Here, a coupled approach between genetic algorithm and finite element method is used. Ebrahimi et al. [12] investigate the design of an actuator with two coupled solenoids. Various coil parameters were investigated using analytical calculations, and optimal design points were found. Another recent work in the area of shape optimization is that of Wang et al. [13]. They also use genetic algorithms and 2D finite element analysis to optimize a coil actuator with multiple objectives. Yongbae et al. [14] use finite element analysis to optimize the response of a linear actuator through parameter studies of individual geometric quantities of the actuator. In one of the most recent works, Abedinifar et al. [15] present a multiobjective optimization approach using a particle swarm algorithm as a means to find a global optimum for a solenoid actuator with respect to a constant and high magnetic force over its working range. In addition to design optimization, coil manufacturing can also be studied, such as by Punnarungsri and Laosiritaworn [16], who use design of experiments to optimize the baking process of coils for a hard disk actuator.

Simple design formulas are commonly used for infinitely long solenoids, but they are not suitable for short coils with small diameters. This study investigates the deviation from simulation results using the finite element software FEMM [17], comparing different design equations considering the length or radius of the solenoid. Note that only static magnetic fields are analyzed.

Furthermore, the design of a solenoid requires the selection of optimal parameters like radius, length, current, or wire gauge. A solenoid comprising a small wire diameter and a correspondingly lower current flow, but numerous turns, can generate a magnetic field of equal strength to a solenoid with fewer turns and a larger current flow.

The main aim of this paper is to utilize design of experiments methodologies to determine the best solenoid parameters, balancing the maximum magnetic field at the center with minimum power consumption and/or coil mass. This is especially significant for solenoids used in vacuum chambers and aerospace applications, where cooling and spatial limitations are crucial. Another application where this is pertinent is reducing the size and power consumption of coils for small integrated devices where space and power are constrained. Additionally, minimizing thermal load serves as a goal for reducing the power consumption of coils. This also has implications in unexpected areas, such as precision machining [18]. The straightforward decrease in copper usage in coils and the resulting reduction in electricity costs from lower power consumption justifies the implementation of these techniques from an economic perspective.

This paper outlines a quick and easily-implemented method for optimizing coils in terms of multiple target variables. This is in contrast to most of the solenoid and actuator optimization work presented in the literature review, which mainly focuses on optimizing either the actuator geometry or the magnetic field topology. The presented techniques allow the optimization of a coil's fundamental parameters with respect to several desired variables. We apply the presented principles to the design of a solenoid for a magnetic nozzle configuration and derive an optimal design. Finally, other potential optimization targets beyond energy, magnetic field, and mass are explored as extensions of the methods presented.

II. MAGNETIC FIELD OF SOLENOIDS

A solenoid is a cylindrical coil of tightly wound wire. Solenoids are utilized to generate adjustable magnetic fields, particularly for producing highly uniform fields. Considering an ideal, infinite solenoid, the magnetic flux density along its axis is easy to describe. It has a constant value of [19]

$$B = \mu_0 \cdot H \tag{1}$$

$$B = \mu_0 \cdot N \cdot \frac{I}{L}\,, \tag{2}$$

where B is the magnetic flux density and N, I and L are the number of turns, coil current and length of the solenoid along its axis, respectively. H is the magnetic field strength with $\mu_0 = 4\pi \cdot 10^{-7}\ \mathrm{kg\,m\,s^{-2}\,A^{-2}}$ as the magnetic vacuum permeability [20].

Since there are no infinitely long coils, this is of course an approximation for any real world application, especially when the length L is of the same order of magnitude as the radius R of the coil. The length may also often be much smaller than the radius of the solenoid, as is the case with coil arrangements such as Helmholtz, Barker, and Braunbek [21], [22], [23]. Solenoids like these with $R \gg L$ are better described by [19]

$$B = \mu_0 \cdot N \cdot \frac{I}{2\bar{R}}\,, \tag{3}$$

where $\bar{R}$ is the solenoid mean radius. Of course, this is also only a reasonable approximation up to a certain combination of coil length and radius, and where precision of estimation can be traded for simplicity of equation (see section III).

For an accurate estimate of the magnetic flux density for a solenoid of any dimension, one can apply the Biot-Savart law

for individual conductor loops [19, p. 772ff.], [24, p. 224ff.]

$$d\vec{B} = \frac{\mu_0}{4\pi}\frac{Id\vec{l}\times\hat{r}}{r^2}\,. \tag{4}$$

An element $d\vec{l}$ along a wire loop with the radius R, carrying a current I in the same direction as $d\vec{l}$, produces a magnetic field $d\vec{B}$ at a point P. The distance from $d\vec{l}$ to P is r with $\hat{r}$ as the unit vector pointing in the same direction (see Fig. 1).

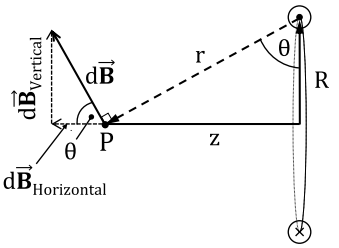

FIGURE 1. Current-carrying wire element producing a magnetic field $d\vec{B}$ at point P according to the Biot-Savart law (based on [24, p. 227]).

Integrating along the loop yields a horizontal and a vertical component of $d\vec{B}$, with the vertical components canceling each other from opposite sides of the loop and the horizontal components combining to give [24, p. 227]

$$\vec{B}(z) = \int d\vec{B}_{horizontal} = \frac{\mu_0}{4\pi} I \int_{wire} \frac{d\vec{l}}{r^2} cos(\theta)\,. \tag{5}$$

Since $d\vec{l}$ and $\hat{r}$ are perpendicular, the constant factor $cos(\theta)$ projects the horizontal components and the integral simplifies to the circumference of the loop, yielding [24, p. 227]

$$B(z) = \frac{\mu_0 I}{4\pi}\frac{cos(\theta)}{r^2}2\pi R = \frac{\mu_0 I}{2}\frac{R^2}{(R^2+z^2)^{3/2}}\,. \tag{6}$$

With (6) for the magnetic flux density along a single loop at a distance z from the center on the axis, B on the axis for the entire solenoid can be readily determined by superposition [25]. This also allows the calculation of the axial magnetic field of several individual coils without resorting to more complex tools such as finite element simulations. For a single layer of windings, (6) can also be integrated to give

$$B(z) = \frac{\mu_0 NI}{2L}\left(\frac{z+\frac{L}{2}}{\sqrt{(z+\frac{L}{2})^2+R^2}} - \frac{z-\frac{L}{2}}{\sqrt{(z-\frac{L}{2})^2+R^2}}\right) \tag{7}$$

as the magnetic flux density on the symmetry axis for a single layer of N turns with length L [26]. From this, (2) can be derived with $L \gg R$, as well as (3) for short solenoids with $R \gg L$, and $z = 0$, respectively.

III. COMPARISON OF ESTIMATES

Equations (2), (3), and (6) provide the means to calculate the peak magnetic flux density along the axis of a solenoid. This allows to determine whether a significantly better estimate of the magnetic flux density can be obtained with (6), and whether the increased computational effort of superposing over all windings is worth it. The results are compared with an analysis using FEMM.

To calculate the total magnetic field using (6), as well as the total conductor length for the power estimation, the inner winding radius and the height difference between each successive winding layer are required. A first approach for the latter would be to simply add the wire diameter to the radius for each layer. However, a more tightly packed coil can be achieved by positioning the top layer in the grooves of the layer below. This most ideal orthocyclic winding will be considered here, knowing that it is very difficult to achieve in practice and also not over the entire circumference due to the layer jump area [27, p. 149ff.]. By idealizing the conductor cross-section as a circle, it can be determined that the optimal center-to-center distance between two layers is

$$\Delta h = \bar{d}\cdot\frac{\sqrt{3}}{2}\,, \tag{8}$$

with the wire gauge $\bar{d}$ including any coating. With this, the magnetic field for the solenoid is calculated by superposing (6) for each loop, increasing the radius by Δh for each layer. For the power calculation, only the pure conductor diameter d_w is used and the total conductor length is calculated assuming no layer jump area in the winding.

Fig. 2 shows the peak flux density B_{max} at the center for different solenoid lengths from 10 mm to 200 mm. The other parameters where kept at 5 A, 1 mm, 15 mm, and 300 for the current, conductor diameter, inner radius, and number of turns, respectively. These parameters are in the order of magnitude as needed for the optimized coil design.

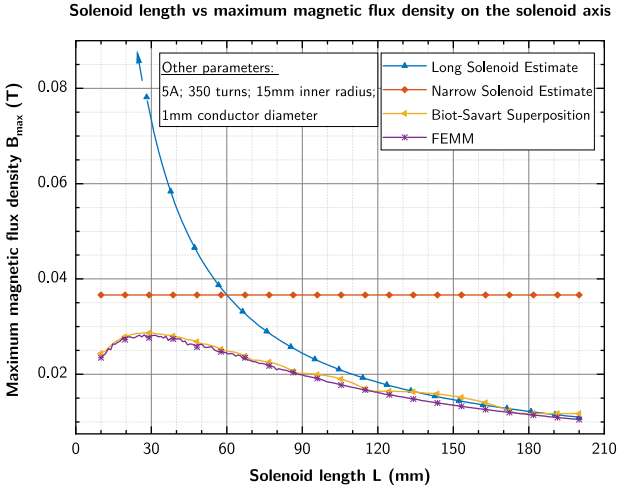

FIGURE 2. Comparison of magnetic flux density maxima, estimated with different equations and finite element analysis in FEMM.

It is evident that (2) overestimates the flux density for short coils, and it only becomes more accurate than (3) when the length is significantly larger than the radius. The superposition of (6) agrees very well with the finite element analysis over the entire plotted range. It should also be noted that there remains some uncertainty in how FEMM distributes the solenoid windings across its cross-section. Slight deviations in the estimate may occur if the windings are evenly distributed across the cross-section for the calculation without physical constraints.

The superposition principle is also not limited to a single solenoid. It requires not much more effort to apply the same formula to a set of coils and get the magnetic flux density at multiple positions across the symmetry axis, not just the maximum flux density as in Fig. 2. Fig. 3 shows the magnetic flux density of two solenoids for a magnetic nozzle calculated using (6) and compared to the corresponding setup evaluated in FEMM, showing good agreement. FEMM shows a slight disparity in magnetic flux density between the left and right halves of the setup. This is despite the expected symmetry of the magnetic field due to the identical coils on both sides, as seen in the results of the analytical calculation. And while the FEMM simulation takes only about a second to run, it is not ideal for optimization because it takes nearly 20 times as long to run compared to the analytical calculation for this example. Therefore, only the latter will be used in the following sections.

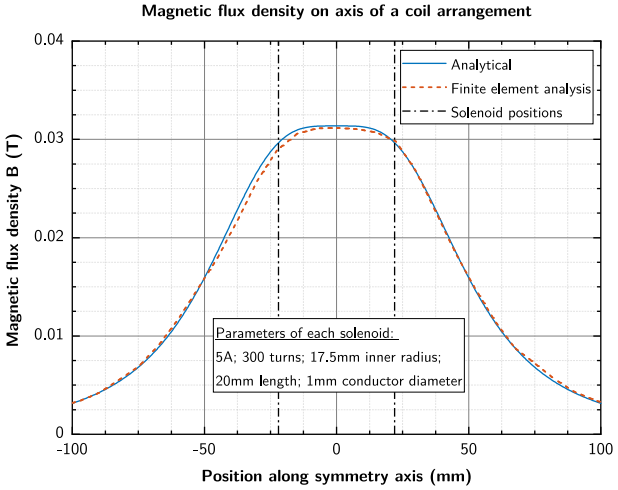

FIGURE 3. Magnetic flux density on axis for a magnetic nozzle configuration; Comparison of results from analytic calculation and finite element analysis.

It is noteworthy that Fig. 2 indicates an optimal length of approximately 25 mm for the given coil parameters. Below this threshold, it is likely that too many layers are needed to fit all the windings onto the solenoid, so that the top layers contribute very little to the overall magnetic flux density. As the length increases, the windings, and thus the flux density, become too widely distributed to produce a high-density field. Of course, the latter may have greater field homogeneity towards the center of its axis. The next sections will deal with the optimization of all parameters, not only the coil length, but also the conductor diameter, the current, the turns, and the inner radius of the solenoid.

IV. DESIGN OF EXPERIMENTS

A. INTRODUCTION

Design of experiments is a set of techniques for observing the output response of a process by changing input variables in a controlled manner while also accounting for uncontrollable noise factors. It is commonly used for experimental design and analysis and process optimization [28], [29].

But a magnetic coil can also be seen as a process or black box that outputs a specific magnetic field for a given set of input variables. The latter are design parameters such as the coil wire diameter, current, and dimensions. Therefore, design of experiments methods are used here to find the most optimal design parameters for a solenoid that maximize the flux density in the center while minimizing the power consumed. Additional optimization objectives such as coil mass or cost can easily be added to the optimization.

As a starting point, consider the model in Fig. 4. Since the process, i.e. the conversion from inputs to magnetic field as output response, is done by evaluating (6), the model has no noise factors in this case. This also means that multiple-response optimization is possible without first creating a metamodel from experimental data that tries to separate random noise from actual effects [28], [29]. Computational time may also motivate the creation of a metamodel. This is often the case with complex simulation models, where techniques such as space mapping can be used to reduce computation time for optimization [30]. For this, the analytical model is superior to finite element analysis, as ascertained in section III, since it can be solved considerably faster. Thus, there is no need for a metamodel, since a large number of factor combinations can be solved quickly.

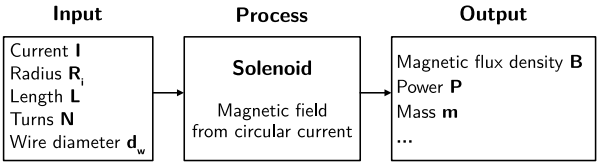

FIGURE 4. Design of experiments model for an idealized solenoid.

B. MULTIPLE-RESPONSE OPTIMIZATION

Each optimization requires a scalar evaluation or valuation function that can be minimized or maximized, respectively. This function relates each of the output variables that are to be optimized to each other. For this purpose, ramp functions or desirability factors q_1 and q_2 were created for the magnetic flux density and the power consumption [28, p. 132f.]

$$q_1 = \begin{cases} 0 & \forall \quad B \le L_1 \\ \left(\dfrac{B - L_1}{T_1 - L_1}\right)^{r_1} & \forall \quad L_1 < B < T_1 \\ 1 & \forall \quad B \ge T_1 \end{cases} \tag{9}$$

$$q_2 = \begin{cases} 1 & \forall \quad P \le T_2 \\ \left(\dfrac{L_2 - P}{L_2 - T_2}\right)^{r_2} & \forall \quad T_2 < P < L_2 \\ 0 & \forall \quad P \ge L_2 \end{cases} \tag{10}$$

with $L_{1,2}$ as the limit and the target value $T_{1,2}$ for the flux density and the power, respectively, as well as $r_{1,2}$ to shape the individual responses.

The goal is to maximize the magnetic flux density while minimizing the power consumption. The range for optimization can be set by choosing suitable boundary

conditions. For the magnetic flux density, a range of $L_1 = 0.03\,\mathrm{T}$ to $T_1 = 0.1\,\mathrm{T}$ was chosen. A weaker magnetic field would no longer be sufficient for the required application, and stronger magnetic fields are not achievable within the power target and solenoid dimensions. The power was restricted to a maximum of $L_2 = 50\,\mathrm{W}$, because more power would become increasingly difficult to cool in a vacuum chamber. The targeted minimum was $T_2 = 0\,\mathrm{W}$. The limits should not be too restrictive in order to leave enough room for the optimization [28, p. 133]. The desirability factors can also be exponentiated to shape the individual responses [28, p. 133f.]. Here, only linear mapping with $r_1 = r_2 = 1$ was used.

Combining q_1 and q_2 into a desirability function is done by taking their geometric mean with n_q as the number of all responses for optimization and k_i as an optional factor of importance for each individual desirability factor q_i [28, p. 133], [31]

$$F = 1 - \left(\prod_{i=1}^{n_q} q_i^{k_i} \right)^{\frac{1}{\sum_i k_i}} . \tag{11}$$

This compact target function can be easily solved using a variety of solvers. Even simple solvers are appropriate for this task [28, p. 133]. To handle multiple local minima, various initial positions are employed in order to discover a global optimum within the parameter space. The 'fmincon' solver paired with Matlab's 'MultiStart' object was utilized for the global minimum search [32]. This is a constrained nonlinear solver for minimizing multivariable functions. The 'interior-point' algorithm was selected due to its ability to effectively handle this type of problem and serve as a suitable starting point for most optimization problems. Notably, the 'interior-point' algorithm does not necessitate an additional gradient to be supplied, unlike the 'trust-region-reflective' algorithm. The objective function, lower and upper bounds were provided, and all remaining options remained at default settings.

For each step of the solver, the objective function selects a point within the parameter space (as shown in the 'Input' section of Fig. 4) and calculates the corresponding output, such as flux density and power. Subsequently, we determine the desirability factor q_i for each output variable and use it to calculate the total desirability F for that specific step, following (11). This output represents the objective function, which is minimized by altering the input parameters.

Each optimization run utilized 1000 starting points within predetermined parameter space boundaries. It was found that this number of starting points was sufficient for all runs, and increasing this did not improve the results. The power was calculated based on a conductivity assumption of pure copper at 20 °C of $59.595\,\mathrm{m\,\Omega^{-1}\,mm^{-2}}$ [33, p. 290].

The results of the optimization runs are presented in the subsequent section.

V. RESULTS

The first run was done with a relatively broad parameter space between the lower and upper bounds for all five input variables. The boundaries are shown in Table 1. The geometric variables were chosen so that the solenoid dimensions would just fit to the rest of the design. Conductor diameter and number of turns were mostly limited by practical considerations. Very small conductor diameters with many turns would result in a very laborious winding process, and a wire thickness beyond the upper limit would be difficult to form into a coil and would significantly increase the outer diameter of the solenoid. The current was limited to 10 A due to power supply and vacuum feedthrough limitations.

TABLE 1. Boundaries of input variables for first optimization run.

Variables	Lower boundary	Upper boundary
Conductor diameter d_w	0.4 mm	2 mm
Current I	1 A	10 A
Inner radius R_i	17.5 mm	30 mm
Windings N	100	500
Length L	15 mm	30 mm

With these limits and the desirability functions (9) to (11), the parameter combinations in Table 2 are found by the solver using multiple starting points, in descending order of desirability, with the first row corresponding to the global minima of F in the context of the optima found.

Note that for all optimization runs presented, the magnetic flux density peak is considered. If a particular field distribution is desired, a different metric must be designed to accommodate it. This could be done, for example, by considering the length within which the magnetic field deviates from the peak by a specified percentage. This could also be used to optimize a combined magnetic field from multiple coils. Here, we focus on a single solenoid with the aim of attaining a high magnetic flux density peak within the power target.

The optimal inner radius is right at the lower boundary of the parameter space. This is, of course, because increasing it reduces the magnetic flux density and lengthens the wire, thereby increasing resistance and power consumption. Increasing it beyond the lower limit of the parameter space is therefore disadvantageous. It is also obvious that large wire diameters are particularly preferred. But there are also solutions with smaller diameters. 2 mm thick wire is already comparatively difficult to wind. For this reason, and based on the initial results, the mass of the solenoid was also taken into account as it has an influence on both the dimensions and indirectly on the material cost. The mass m was included in (11) using

$$q_3 = \begin{cases} 1 & \forall \quad m \leq T_3 \\ \left(\dfrac{L_3 - m}{L_3 - T_3} \right)^{r_3} & \forall \quad T_3 < m < L_3 \\ 0 & \forall \quad m \geq L_3 \end{cases} \tag{12}$$

with $T_3 = 0\,\mathrm{kg}$ and $L_3 = 1\,\mathrm{kg}$. The weights $r_{1\ldots3}$ and importance factors $k_{1\ldots3}$ were set to unity for all response variables in all runs. In addition, the current was limited to 6 A in order to leave enough headroom to allow the possibility of

TABLE 2. Results of first optimization run for magnetic flux density peak and consumed power[1].

d_w (mm)	I (A)	R_i (mm)	N	L (mm)	B (mT)	Power (W)	Mass (kg)
1.84	7.81	17.7	338	29.0	45.2	29.3	1.83
1.90	9.38	18.0	259	28.0	43.9	27.8	1.39
1.78	7.21	17.8	351	28.1	43.3	27.9	1.79
1.91	8.74	17.9	318	28.2	46.8	32.8	1.93
1.90	9.84	18.2	238	26.0	43.0	28.5	1.28
1.82	6.58	18.0	403	28.8	42.4	27.9	2.36
1.80	7.96	18.2	293	26.6	41.4	26.5	1.47
1.85	6.71	17.7	451	29.3	46.1	33.4	2.94
1.92	7.16	17.9	393	28.2	43.6	30.5	2.68
1.67	6.03	18.4	429	28.4	42.4	28.6	2.07

[1]Only the best 10 results are shown and rounded to reasonable precision, depending on the parameter.

increasing the magnetic flux density for short periods of time. Thus, the final optimization run yielded the results shown in Table 3.

TABLE 3. Results of final optimization run for magnetic flux density peak, consumed power and mass[1].

d_w (mm)	I (A)	R_i (mm)	N	L (mm)	B (mT)	Power (W)	Mass (kg)
0.92	5.41	17.6	311	23.5	41.0	34.0	0.28
0.96	5.98	17.5	257	22.2	38.3	31.1	0.24
0.93	4.94	17.6	343	21.7	40.1	32.1	0.34
1.02	5.99	17.8	305	23.5	42.8	35.3	0.35
0.89	4.47	17.5	387	20.7	40.8	33.6	0.35
1.01	5.71	17.7	298	20.0	40.0	32.9	0.35
1.01	5.9	17.7	272	18.9	38.4	31.6	0.32
0.86	4.81	17.5	316	18.2	37.6	32.6	0.26
0.99	5.47	18.0	302	20.7	38.7	31.4	0.34
0.99	5.58	17.9	303	19.7	39.5	33.0	0.35

[1]Only the best 10 results are shown and rounded to reasonable precision depending on the parameter.

These results describe solenoids which are much easier to handle in terms of size and mass, and whose performance does not differ much from the results presented in Table 2. It is also evident, that many solutions are basically the same, considering that the manufacturing tolerances of some parts are greater than the differences of a few tens of millimeters between some solutions. Also, not all wire diameters are available off the shelf. Therefore, Table 4 presents practical solutions derived from the theoretical results. The selection of wire diameters is based on the availability of coated coil wire from various manufacturers.

All solutions found in the final optimization run are in the same region of the parameter space. Therefore, for initial runs or for systems that are not well known, care should be taken not to restrict the parameter space too much. By performing a coarse sweep with a wide parameter space, trends can be observed. These can help to find an optimal design. With this knowledge, the parameter space can then be adjusted by setting the corresponding limits. It is recommended to conduct initial runs using linear weighting for better trend visibility. Additionally, unless the system is very well known, it is advisable not to vary the weighting and the importance

TABLE 4. Summarized practical results of the final optimization output for optimized magnetic flux density peak, power consumption and coil mass.

d_w (mm)	I (A)	R_i (mm)	N	L (mm)	B (mT)	Power (W)	Mass (kg)
0.90	5.4	17.5	310	23.5	41.0	34.98	0.26
0.90	4.5	17.5	390	22.0	41.2	33.01	0.36
0.95	6.0	17.5	260	22.0	38.6	32.57	0.25
1	5.5	17.5	300	21.0	39.3	30.48	0.34
1	5.8	17.5	280	20.0	39.1	31.49	0.31
1	6.0	17.5	300	23.5	42.8	35.21	0.33

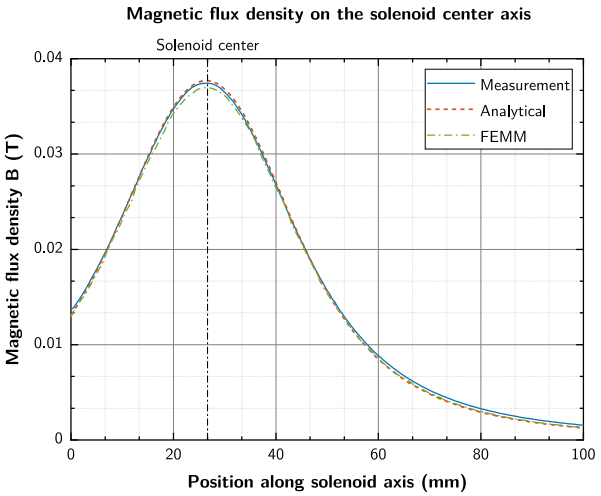

FIGURE 5. Magnetic flux density on the solenoid center axis - comparison between measurement, analytical calculation and finite element simulation.

factor at the same time, as the interaction of both factors is very complex and makes the interpretation of the results difficult.

Based on the results presented in Table 4, the solution with a wire diameter of 1 mm, 300 turns, and approximately 5.5 A of current was selected for practical implementation due to its low power consumption relative to other solutions in Table 4.

The flux density of the solenoid manufactured with these parameters was also measured and compared with the result of (6) and a finite element simulation. Fig. 5 shows the measured magnetic flux density on the center axis compared to the analytical value and the results from FEMM. The measurement was done with an MLX90393 hall effect sensor. All values agree very well and the deviations are within the expected margin of error. This also shows that the applied method of calculating the magnetic flux density by superposing each individual winding at different positions along a solenoid axis provides a reasonably simple and fast method of accurately calculating the magnetic field strength on the axis of cylindrical solenoids. With the appropriate modifications of (6), this should also be the case for rectangular coils or coils of other cross-sections.

It is also possible to generate response surface plots for F for different combinations of two parameters while holding the others constant. If some variables are already fixed by other design choices, these can be useful to quickly and easily narrow down on the subdomain of the remaining parameter space with the highest desirability. A collection

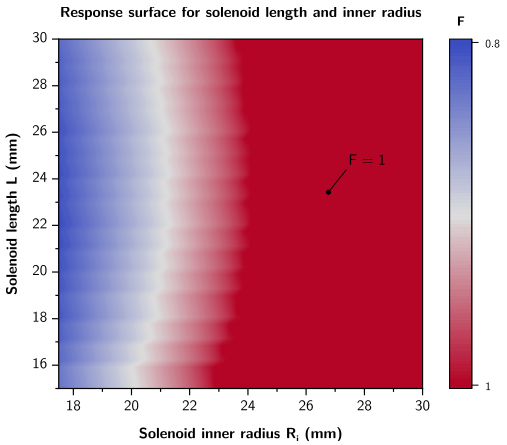

FIGURE 6. Surface response plot for solenoid length and inner radius; Other parameters: 1 mm wire diameter, 5 A, 300 turns.

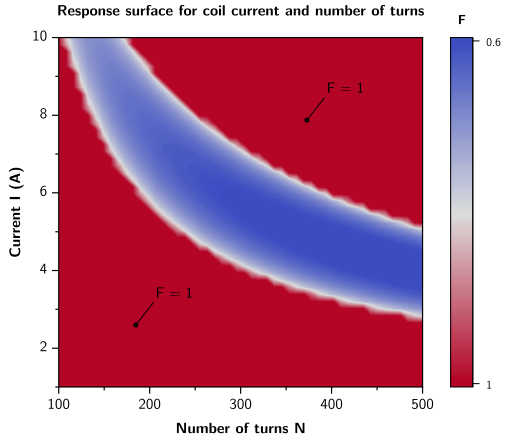

FIGURE 7. Surface response plot for coil current and number of turns; Other parameters: 1 mm wire diameter, 17.5 mm radius, 20 mm length.

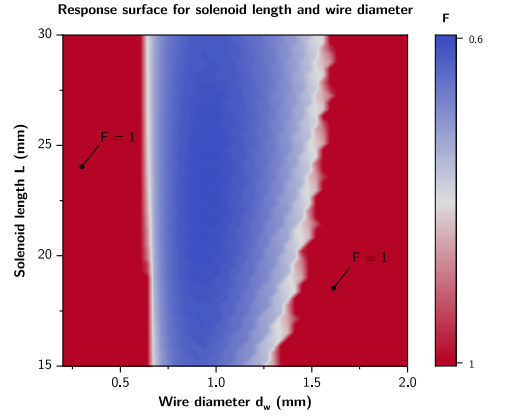

FIGURE 8. Surface response plot for coil length and wire gauge; Other parameters: 5 A, 17.5 mm inner radius, 300 turns.

of response surface plots showing interesting trends for the selected parameter combinations of the solenoid optimized in this section can be found in the Appendix A. These response surfaces were generated with only the flux density and power consumption included in (11) and with linear weighting. Note that small values of F show the highest desirability, since equation (11) is formulated as a minimization problem.

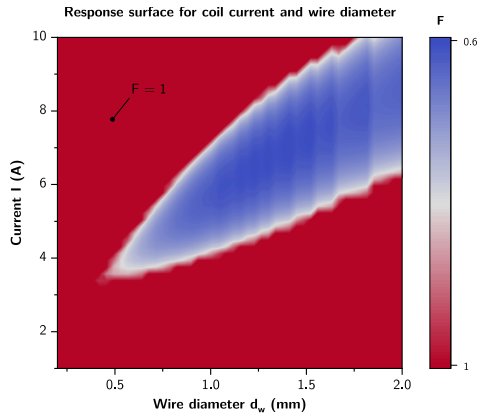

FIGURE 9. Surface response plot for coil current and wire gauge; Other parameters: 17.5 mm inner radius, 20 mm length, 300 turns.

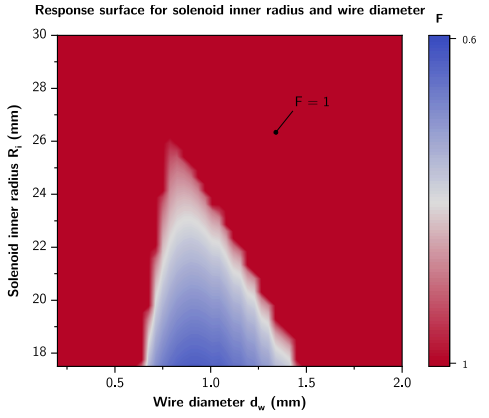

FIGURE 10. Surface response plot for solenoid inner radius and wire gauge; Other parameters: 5 A, 20 mm length, 300 turns.

VI. CONCLUSION

To optimize a solenoid for high flux density, low power consumption, and additionally low overall mass, design of experiments and, in particular, multiple-response analysis were used. First, an equation was introduced to quickly and accurately calculate the expected magnetic flux density on the axis of an ideal solenoid. The results were compared with simpler predictions and finite element analysis. A desirability function was then established as a minimization problem to optimize the conductor diameter, current, solenoid inner radius and length, and number of windings for the specified output responses. Finally, an optimal parameter combination was selected from the calculated results. Magnetic flux density measurements showed very good agreement with the calculations.

The presented method has been successfully applied to the optimization of solenoids in a two-coil magnetic nozzle assembly. It provides a straightforward way to optimize virtually unlimited parameters to different objective values, and also allows for easy adjustment of weights and importance factors between all objectives. In this case, a solenoid was optimized to achieve high magnetic flux density while minimizing both power consumption and mass within the selected parameter space. A possible further development of

the concept would be to include the uniformity of the magnetic field over a certain distance along the coil axis. This can be useful for certain Helmholtz-like arrangements. It may also be that for large coils, aluminum wire is better suited for an optimal balance of power consumption and mass. This can also be readily analyzed with the methodology presented. It is also conceivable that the heating of the coil during prolonged operation is taken into account and a temperature-dependent resistivity is used to calculate the power.

APPENDIX A
RESPONSE SURFACE PLOTS

See Figs. 6–10.

REFERENCES

[1] P. Eyabi and G. Washington, "Modeling and sensorless control of an electromagnetic valve actuator," *Mechatronics*, vol. 16, nos. 3–4, pp. 159–175, Apr. 2006.

[2] K. W. Lim, N. C. Cheung, and M. F. Rahman, "Proportional control of a solenoid actuator," in *Proc. 20th Annu. Conf. IEEE Ind. Electron. (IECON)*, vol. 3, Sep. 1994, pp. 2045–2050.

[3] Y. Mitsutake, K. Hirata, and Y. Ishihara, "Dynamic response analysis of a linear solenoid actuator," *IEEE Trans. Magn.*, vol. 33, no. 2, pp. 1634–1637, Mar. 1997.

[4] N. D. Vaughan and J. B. Gamble, "The modeling and simulation of a proportional solenoid valve," *J. Dyn. Syst., Meas., Control*, vol. 118, no. 1, pp. 120–125, Mar. 1996.

[5] X. Xu, X. Han, Y. Liu, Y. Liu, and Y. Liu, "Modeling and dynamic analysis on the direct operating solenoid valve for improving the performance of the shifting control system," *Appl. Sci.*, vol. 7, no. 12, p. 1266, Dec. 2017.

[6] Y. Xu and B. Jones, "A simple means of predicting the dynamic response of electromagnetic actuators," *Mechatronics*, vol. 7, no. 7, pp. 589–598, Oct. 1997.

[7] M. Yang, J. Zhang, and B. Xu, "Experimental study and simulation analysis on electromagnetic characteristics and dynamic response of a new miniature digital valve," *Adv. Mater. Sci. Eng.*, vol. 2018, no. 1, pp. 1–8, Jan. 2018.

[8] F. Mach, I. Nový, P. Karban, and I. Doležel, "Shape optimization of electromagnetic actuators," in *Proc. ELEKTRO*, May 2014, pp. 595–598.

[9] J. Hey, T. J. Teo, V. P. Bui, G. Yang, and R. Martinez-Botas, "Electromagnetic actuator design analysis using a two-stage optimization method with coarse–fine model output space mapping," *IEEE Trans. Ind. Electron.*, vol. 61, no. 10, pp. 5453–5464, Oct. 2014.

[10] S. L. Lalitha and R. C. Gupta, "The mechanical design optimization of a high field HTS solenoid," *IEEE Trans. Appl. Supercond.*, vol. 25, no. 3, pp. 1–4, Jun. 2015.

[11] E. Plavec and M. Vidovic, "Genetic algorithm based plunger shape optimization of DC solenoid electromagnetic actuator," in *Proc. 24th Telecommun. Forum (TELFOR)*, Nov. 2016, pp. 1–4.

[12] N. Ebrahimi, P. Schimpf, and A. Jafari, "Design optimization of a solenoid-based electromagnetic soft actuator with permanent magnet core," *Sens. Actuators A, Phys.*, vol. 284, pp. 276–285, Dec. 2018.

[13] S. J. Wang, Z. D. Weng, B. Jin, and H. X. Cai, "Multi-objective genetic algorithm optimization of linear proportional solenoid actuator," *J. Brazilian Soc. Mech. Sci. Eng.*, vol. 43, no. 2, pp. 1–11, Feb. 2021.

[14] K. Yongbae, P. Chansol, and K. Youngil, "Optimal design of uni-directional linear solenoid," in *Proc. 6th Int. Conf. Electric Power Equip.-Switching Technol. (ICEPE-ST)*, Mar. 2022, pp. 376–379.

[15] M. Abedinifar, S. Ertugrul, and G. T. Tayyar, "Design optimization of a solenoid actuator using particle swarm optimization algorithm with multiple objectives," *Adv. Mech. Eng.*, vol. 14, no. 11, Nov. 2022, Art. no. 168781322211357.

[16] P. Punnarungsri and W. Laosiritaworn, "Optimization of coil baking parameters using design of experiments," in *Proc. Int. MultiConf. Eng. Comput. Scientists*, in Lecture Notes in Engineering and Computer Science, vol. 2, Hong Kong, 2013, pp. 1–5.

[17] D. C. Meeker. *Finite Element Method Magnetics (Version 4.2)*. Accessed: Aug. 13, 2024. [Online]. Available: https://www.femm.info

[18] J. Mayr, J. Jedrzejewski, E. Uhlmann, M. Alkan Donmez, W. Knapp, F. Härtig, K. Wendt, T. Moriwaki, P. Shore, R. Schmitt, C. Brecher, T. Würz, and K. Wegener, "Thermal issues in machine tools," *CIRP Ann.*, vol. 61, no. 2, pp. 771–791, 2012.

[19] R. A. Serway and J. W. Jewett, *Physics for Scientists Engineers With Modern Physics*, 10th ed., Melbourne, VIC, Australia: Cengage, 2019.

[20] P. J. Mohr, D. B. Newell, B. N. Taylor, and E. Tiesinga. (May 20, 2019). *The NIST Reference on Constants, Units and Uncertainty: Fundamental Physical Constants*. [Online]. Available: https://physics.nist.gov/cuu/Constants/index.html

[21] J. C. Maxwell, *A Treatise on Electricity and Magnetism*, vol. 1, 3rd ed., New York, NY, USA: Dover, 1961.

[22] J. R. Barker, "New coil systems for the production of uniform magnetic fields," *J. Sci. Instrum.*, vol. 26, no. 8, pp. 273–275, Aug. 1949.

[23] W. Braunbek, "Die erzeugung weitgehend homogener magnetfelder durch kreisströme," *Zeitschrift Für Physik*, vol. 88, nos. 5–6, pp. 399–402, 1934.

[24] D. J. Griffiths, *Introduction to Electrodynamics*, 3rd ed., Upper Saddle River, NJ, USA: Prentice-Hall, 1999.

[25] K. Foelsch, "Magnetfeld und Induktivität einer zylindrischen spule," *Archiv Für Elektrotechnik*, vol. 30, no. 3, pp. 139–157, Mar. 1936.

[26] N. Derby and S. Olbert, "Cylindrical magnets and ideal solenoids," *Amer. J. Phys.*, vol. 78, no. 3, pp. 229–235, Mar. 2010.

[27] J. Hagedorn, F. Sell-Le Blanc, and J. Fleischer, *Handbuch Der Wickeltechnik Für Hocheffiziente Spulen Und Motoren*. Berlin, Germany: Springer, 2016.

[28] K. Siebertz, D. van Bebber, and T. Hochkirchen, *Statistische Versuchsplanung*. Berlin, Germany: Springer, 2010.

[29] D. C. Montgomery, *Design and Analysis of Experiments*, 8th ed., Hoboken, NJ, USA: Wiley, 2013.

[30] J. W. Bandler, Q. S. Cheng, S. A. Dakroury, A. S. Mohamed, M. H. Bakr, K. Madsen, and J. Sondergaard, "Space mapping: The state of the art," *IEEE Trans. Microw. Theory Techn.*, vol. 52, no. 1, pp. 337–361, Jan. 2004.

[31] H. Akçay and A. S. Anagün, "Multi response optimization application on a manufacturing factory," *Math. Comput. Appl.*, vol. 18, no. 3, pp. 531–538, Dec. 2013.

[32] MathWorks, Inc. (2021). *Matlab (Version 2021b)*. [Online]. Available: https://mathworks.com/

[33] N. A. Lange, *Lange's Handbook of Chemistry* (McGraw-Hill Handbook), 15th ed., New York, NY, USA: McGraw-Hill, 1999.

CHRISTOPH PETER was born in Lauchhammer, Germany, in 1995. He received the Diploma degree in mechanical engineering (aerospace engineering) from the University of Technology Dresden (TU Dresden), Germany, in 2021, where he is currently pursuing the Ph.D. degree in mechanical engineering.

Since 2021, he has been a Research Assistant with the Institute of Aerospace Engineering, TU Dresden. His research interests include the development of a miniature electric propulsion system for micro- and nanosatellites and the utilization of novel fuels in electric propulsion systems.

MARTIN TAJMAR studied physics, space, and electrical engineering and graduated with a Ph.D. in 1999 from Vienna University of Technology Austria.

After research stays at NASA JPL and ESA-ESTEC, he joined Austrian Institute of Technology, from 2000 to 2010, where he was the Head of the Business Unit Space Propulsion and Advanced Concepts. After being appointed as an Associate Professor with KAIST, he moved to TU Dresden, Germany, as a Full Professor and the head of the Chair of Space Systems, in 2012, where he was later appointed as the Director of the Institute of Aerospace Engineering. Besides the developments of his group, which include small satellites and activities on liquid-fueled rocket engines using aerospike nozzles. He has published 115 journal articles, 235 conference papers, one book, and three book chapters. His research interests include the development of novel electric propulsion systems and advanced concepts for future space flight.